

Robust Pseudo-label Learning with Neighbor Relation for Unsupervised Visible-Infrared Person Re-Identification

Xiangbo Yin
School of Informatics, Xiamen
University
xiangboyin@stu.xmu.edu.cn

Jiangming Shi
Institute of Artificial Intelligence,
Xiamen University
jiangming.shi@outlook.com

Yachao Zhang
Tsinghua Shenzhen International
Graduate School, Tsinghua University
yachaozhang@sz.tsinghua.edu.cn

Yang Lu
School of Informatics, Xiamen
University
luyang@xmu.edu.cn

Zhizhong Zhang
East China Normal University
zzzhang@cs.ecnu.edu.cn

Yuan Xie*
East China Normal University
yxie@cs.ecnu.edu.cn

Yanyun Qu*
School of Informatics, Xiamen
University
yyqu@xmu.edu.cn

ABSTRACT

Unsupervised Visible-Infrared Person Re-identification (USVI-ReID) presents a formidable challenge, which aims to match pedestrian images across visible and infrared modalities without any annotations. Recently, clustered pseudo-label methods have become predominant in USVI-ReID, although the inherent noise in pseudo-labels presents a significant obstacle. Most existing works primarily focus on shielding the model from the harmful effects of noise, neglecting to calibrate noisy pseudo-labels usually associated with hard samples, which will compromise the robustness of the model. To address this issue, we design a Robust Pseudo-label Learning with Neighbor Relation (RPNR) framework for USVI-ReID. To be specific, we first introduce a straightforward yet potent Noisy Pseudo-label Calibration module to correct noisy pseudo-labels. Due to the high intra-class variations, noisy pseudo-labels are difficult to calibrate completely. Therefore, we introduce a Neighbor Relation Learning module to reduce high intra-class variations by modeling potential interactions between all samples. Subsequently, we devise an Optimal Transport Prototype Matching module to establish reliable cross-modality correspondences. On that basis, we design a Memory Hybrid Learning module to jointly learn modality-specific and modality-invariant information. Comprehensive experiments conducted on two widely recognized benchmarks, SYSU-MM01 and RegDB, demonstrate that RPNR outperforms the current state-of-the-art GUR with an average Rank-1 improvement of 10.3%. The source codes will be released soon.

KEYWORDS

USVI-ReID, Noisy Labels, Neighbor Relation Learning, Optimal Transport

1 INTRODUCTION

With the increasing demand for intelligent security, smart monitoring sensor devices for 24-hour surveillance are becoming more prevalent [25, 34, 36, 44, 49, 55]. Due to the different imaging

principles of sensor devices during the daytime and nighttime, the data exhibits multi-modality characteristics, sparking interest in research on visible-infrared person re-identification (VI-ReID). VI-ReID aims to accurately search the special visible/infrared pedestrian images when given a query pedestrian image from another modality, but the significant gap between the two modalities presents a considerable challenge for this task. Existing VI-ReID methods [10, 11, 16, 38, 45, 52, 54] mitigate cross-modality disparities through deep learning, achieving significant performance improvements. However, these methods rely on well-annotated cross-modality data, which is time-consuming and labor-intensive in practical scenarios. Therefore, increasing attention is being drawn to unsupervised visible-infrared person re-identification (USVI-ReID).

The key challenges of the USVI-ReID are obtaining robust pseudo-labels and establishing reliable cross-modality correspondences. Existing USVI-ReID methods [4, 23, 40, 42] mostly follow the DCL [43] framework, which generates pseudo-labels using DBSCAN and establishes cross-modality correspondences based on pseudo-labels. Since pseudo-labels are generated by clustering, they inevitably contain noise. The noisy pseudo-labels may cause the model to incorrectly learn the data distributions and feature representations. To mitigate the effects of the noisy pseudo-labels, DPIS [26] computes the confidence scores of pseudo-labels by analyzing their classifier loss, then uses confidence scores to mitigate the impact of noisy pseudo-labels. PGM [40] reduces the impact of noisy labels by alternately using two unidirectional metric losses, preventing the rapid formation of noisy pseudo-labels. However, these methods don't calibrate noisy pseudo-labels to clear ones, which makes it difficult for the model to exploit hard-to-discriminate features. In order to establish cross-modality correspondences, OTLA [31] utilizes unsupervised domain adaptation to generate pseudo-labels for the infrared images. With the aid of richly annotated visible images, it proposes an optimal transport strategy to allocate pseudo-labels from the visible modality to the infrared modality. However, OTLA adopts the strategy of independently assigning pseudo-labels to each infrared image, which is a massive task with many distractors, leading to unreliable cross-modality correspondences.

*Corresponding author.

In this paper, we propose the Robust Pseudo-Label Learning with Neighbor Relation (RPNR) framework, a unified approach aimed at addressing noisy pseudo-labels and cross-modality correspondences for USVI-ReID. To be specific, to calibrate noisy pseudo-labels, we design two critical modules: Noisy Pseudo-label Calibration (NPC) and Neighbor Relation Learning (NRL). Unlike previous methods that only reduce the effect of noisy pseudo-labels, NPC directly calibrates them. NPC obtains robust prototypes through reliable neighbor samples and calibrates pseudo-labels based on similarity to these prototypes. The significant intra-class variations will hinder the noisy pseudo-label calibration. NRL is proposed to reduce intra-class variations by interacting across all images. NRL promotes the model to cluster closely with neighbor samples, as neighbor samples are often related. In order to establish reliable cross-modality correspondences, we also design two critical modules: Optimal Transport Prototype Matching (OTPM) and Memory Hybrid Learning (MHL). Unlike OTLA, which overlooks the intra-class information and treats all images as separate instances for establishing cross-modality correspondences, OTPM employs intra-class information to build cross-modality correspondences. In brief, OTPM obtains the prototype by clustering and establishes cross-modality correspondences based on these prototypes, instead of all instances. Furthermore, the significant cross-modality gaps will hinder the establishment of cross-modality correspondences. MHL is designed to learn both modality-specific and modality-invariant information by blending two modality-specific memories, effectively bridging the substantial gaps between different modalities.

In conclusion, the main contributions of our method can be summarized as follows:

- We propose the Robust Pseudo-Label Learning with Neighbor Relation (RPNR) framework to address both noisy pseudo-labels and noisy cross-modality correspondences problems in USVI-ReID.
- Two critical modules: Noisy Pseudo-label Calibration (NPC) and Neighbor Relation Learning (NRL) are introduced to obtain robust pseudo-labels.
- Two critical modules: Optimal Transport Prototype Matching (OTPM) and Memory Hybrid Learning (MHL) are introduced to establish reliable cross-modality correspondences.
- Experiments on SYSU-MM01 and RegDB datasets demonstrate the superiority of our method compared with existing USVI-ReID methods, and RPNR generates higher-quality pseudo-labels than other methods.

2 RELATED WORK

2.1 Unsupervised Single-Modality Person ReID

Unsupervised single-modality person ReID aims to learn discriminative identity features from unlabeled person ReID datasets. Existing mainstream purely unsupervised methods primarily rely on pseudo-labels, which involve an iterative process alternating between pseudo-label generation and representation learning [6, 8, 12, 32, 33, 51, 53, 57, 62]. Cluster-Contrst [8] presents a cluster contrast framework, which stores unique centroid representations and performs contrastive learning at the cluster level. Additionally, the momentum update strategy is introduced to reinforce the cluster-level feature consistency in the embedding space. However, a uni-proxy

for a cluster may introduce bias. To address this issue, multi-proxies methods [39, 61] have been proposed to compensate for the shortcomings of uni-proxy approaches. Pseudo-labels inherently contain a portion of noise. To address this issue, label refinement methods [5, 6, 56] are proposed to collect more reliable pseudo-labels. While the aforementioned methods have shown promising results in unsupervised ReID tasks, applying them directly to unsupervised VI-ReID scenarios poses a significant challenge due to the substantial cross-modality gap.

2.2 Unsupervised Visible-Infrared Person ReID

There has been an escalating interest in unsupervised visible-infrared person re-identification (USVI-ReID) owing to its potential to learn modality-specific and modality-invariant information without necessitating cross-modality annotations. Existing mainstream USVI-ReID methods [4, 15, 23, 24, 40, 42] predominantly adhere to the DCL [43] learning framework, which involves two key steps: (1) generating pseudo-labels using a clustering algorithm, and (2) establishing cross-modality correspondences based on these pseudo-labels. PGM [40] and MBCCM [15] perform multi-stage graph matching via building bipartite graphs. OTLA [31] and DOTLA [4] employ the Optimal Transport strategy to assign pseudo-labels from one modality to another modality at the instance level. However, pseudo-labels inevitably contain noise, which may lead to unreliable cross-modality correspondences under the supervision of noisy pseudo-labels. Therefore, there is a need to seek more reliable pseudo-labels for the USVI-ReID task.

2.3 Learning with Noisy Labels

The presence of label noise has been demonstrated to adversely affect the training of deep neural networks [29, 46, 63]. Existing methods devised for handling noisy labels can be primarily categorized into the following two classes: label correction and sample selection. Label correction methods [2, 27, 30, 59] endeavor to utilize the model predictions to rectify the noisy labels. [14] proposes an iterative learning framework SMP to relabel the noisy samples and train the network on the real noisy dataset without using extra clean supervision. [50] utilizes back-propagation to probabilistically update and correct image labels beyond updating the network parameters. Different from label correction methods, sample selection methods [13, 19, 35] aim to select clean samples while discarding noisy samples during the training stage. NCE [18] filters the clean samples according to the neighbor information. CBS [20] proposes to employ confidence-based sample augmentation to enhance the reliability of selected clean samples. For the USVI-ReID task, pseudo-labels generated by the clustering algorithm inevitably contain noise. Therefore, calibrating these noisy pseudo-labels is crucial for improving the performance of USVI-ReID.

3 METHODOLOGY

3.1 Notation Definition

Given an unlabeled visible-infrared person re-identification dataset $\mathcal{D} = \{\mathcal{D}^{\mathcal{V}}, \mathcal{D}^{\mathcal{R}}\}$, where $\mathcal{D}^{\mathcal{V}} = \{x_i^{\mathcal{V}} \mid i = 1, 2, \dots, N^{\mathcal{V}}\}$ represents the unlabeled visible dataset with $N^{\mathcal{V}}$ samples and $\mathcal{D}^{\mathcal{R}} = \{x_i^{\mathcal{R}} \mid i = 1, 2, \dots, N^{\mathcal{R}}\}$ represents the unlabeled infrared dataset with $N^{\mathcal{R}}$

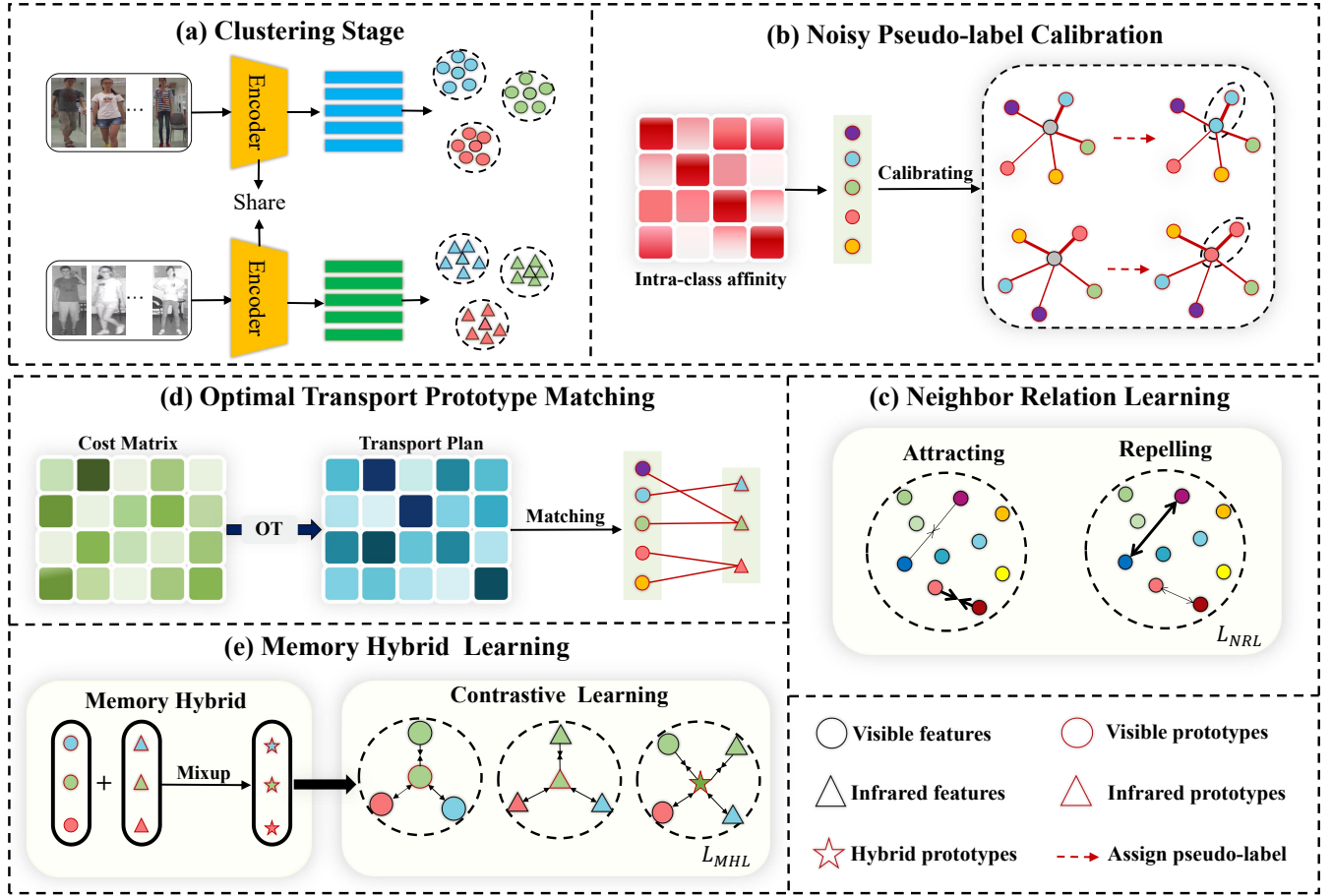


Figure 1: Overall of the proposed RPNR (best viewed in color). Given unlabeled visible-infrared data, RPNR first generates modality-specific pseudo-labels by DBSCAN at stage (a). After that, RPNR calibrates noisy pseudo-labels (grey dots) to obtain robust pseudo-labels (color dots) at stage (b), while modeling potential interactions between all samples (the strength is indicated by thickness) to reduce intra-class variation at stage (c). Additionally, based on the robust pseudo-labels, RPNR employs the optimal transport to establish cross-modality correspondences at stage (d). Finally, with the recast aligned pseudo-labels, RPNR mixes two modality-specific memories as a new hybrid memory to learn both modality-specific and modality-invariant information through contrastive loss at stage (e).

samples. For the USVI-ReID task, the objective is to train a robust model f_θ to project a sample x_i^t from \mathcal{D} into an embedding space \mathcal{F} , where $t = \{v, r\}$. Thus, we can employ the encoder f_θ to extract visible features $F^v = \{f_i^v \mid i = 1, 2, \dots, N^v\}$ and infrared features $F^r = \{f_i^r \mid i = 1, 2, \dots, N^r\}$, where $f_i^t \in \mathbb{R}^d$.

3.2 Overview

The overall framework of the proposed method is shown in Fig. 1. We first employ the DBSCAN [9] algorithm to cluster visible and infrared features. After clustering, we can obtain pseudo-labels $y_i^t \in \{1, 2, \dots, Y^t\}$ of i -th images from modality t , where Y^t is the number of clusters and $t = \{v, r\}$. Since pseudo-labels inevitably contain noise, we first propose a Noisy Pseudo-label Calibration (NPC) module to calibrate noisy labels to obtain more robust pseudo-labels. Afterward, we assign these calibrated pseudo-labels \hat{y}_i^t for

each sample to obtain the “labeled” dataset $\tilde{\mathcal{D}}^V = \{(x_i^v, \hat{y}_i^v)\}_{i=1}^{N^v}$ and $\tilde{\mathcal{D}}^R = \{(x_i^r, \hat{y}_i^r)\}_{i=1}^{N^r}$. However, NPC overlooks the possible interactions between all samples. To make up for this deficiency, we propose a Neighbor Relation Learning (NRL) module, which is designed to model the intricate interactions spanning across all samples. Furthermore, the pseudo-labels generated by two separate clustering for visible and infrared samples reveal a misalignment. To align correspondences between visible and infrared samples, we design an Optimal Transport Prototype Matching (OTPM) module, which considers cross-modality correspondences as alignment between visible and infrared prototypes by optimal transport. Learning modality-invariant features is crucial in cross-modality correspondences. To better mine the modality-invariant information and alleviate significant cross-modality gaps, we propose a Memory Hybrid Learning (MHL) module, which mixes aligned visible

and infrared prototypes as new modality-hybrid prototypes for contrastive learning.

3.3 Noisy Pseudo-label Calibration

Since pseudo-labels are generated by clustering, they inevitably contain noise. We introduce the Noisy Pseudo-label Calibration (NPC) module to correct noisy pseudo-labels. Specifically, given the c -th cluster from modality t , corresponding to a set of d -dimensional features $\{f_{c,i}^t\}_{i=1}^{n_c}$, where n_c denotes the number of features belonging to c -th cluster and $t \in \{v, r\}$. We employ the *Jaccard Similarity* to model the affinity matrix \mathcal{S} of intra-class samples as follows:

$$S_{ij}^t = \frac{|\mathcal{R}(f_{c,i}^t, \kappa) \cap \mathcal{R}(f_{c,j}^t, \kappa)|}{|\mathcal{R}(f_{c,i}^t, \kappa) \cup \mathcal{R}(f_{c,j}^t, \kappa)|}, \quad (1)$$

where S_{ij}^t is the affinity between $f_{c,i}^t$ and $f_{c,j}^t$, and $\mathcal{R}(f_{c,i}^t, \kappa)$ is the κ -reciprocal nearest neighbors of $f_{c,i}^t$. The larger S_{ij}^t , the higher similarity between $f_{c,i}^t$ and $f_{c,j}^t$. For a specific $f_{c,i}^t$, if it is surrounded by more similar samples, the sample is more likely to be reliable. To select reliable samples for a cluster, we design a Similarity Counter G_c^t for each sample:

$$G_{c,i}^t = \sum_{j=1}^{n_c} \text{sign}(S_{ij}^t - \rho), i \in \{1, 2, \dots, n_c\}, \quad (2)$$

where $\text{sign}(\cdot)$ is a *sign* function and ρ is a threshold fixed to 0.5. We can find that correctly categorized samples should have higher similarity counts, so we regard the samples with the top- K similarity counts as reliable samples:

$$id = \arg \max_K G_c^t, \quad (3)$$

where id denotes the indexes of top- K similarity counts.

Then we can obtain a robust prototype with these reliable samples for the c -th cluster:

$$p_c^t = \frac{1}{K} \sum_{i \in id} f_{c,i}^t. \quad (4)$$

After that, we can own a prototype set $p^t = \{p_1^t, p_2^t, \dots, p_{Y^t}^t\}$. For a given sample x_i^t from \mathcal{D}^t , the similarity score $\delta_{c,i}^t$ between the extracted feature f_i^t and the c -th cluster is calculated as follows:

$$\delta_{c,i}^t = \frac{(f_i^t) \cdot (p_c^t)^T}{\|f_i^t\|_2 \cdot \|p_c^t\|_2}, \quad (5)$$

where $\delta_{c,i}^t$ denotes the cosine similarity between the extracted feature f_i^t and the c -th cluster. Larger $\delta_{c,i}^t$ indicates the sample x_i^t is more likely to belong to the c -th cluster. Then, we can obtain the corrected pseudo-label by:

$$\hat{y}_i^t = \arg \max_c \delta_{c,i}^t, c \in \{1, 2, \dots, Y^t\}. \quad (6)$$

Afterward, we assign these corrected labels for each sample for network training.

3.4 Neighbor Relation Learning

Considering high intra-class variability profoundly hampers the NPC module, we propose the Neighbor Relation Learning (NRL) module, which is designed to reduce intra-class variability through the intricate interactions spanning across all pair-wise samples. Following [17], we employ Relaxed Contrastive Loss for learning semantic embedding of pair-wise samples. For convenience, we only explain the process of visible samples. Given a pair of samples (f_i^v, f_j^v) , we compute the Euclidean distance between them by:

$$d_{ij}^v = \|f_i^v - f_j^v\|_2. \quad (7)$$

Then, the visible loss of the NRL module can be formulated:

$$L_{NRL}^v = \underbrace{\frac{1}{N_B} \sum_{i=1}^{N_B} \sum_{j=1}^{N_B} \omega_{ij}^v d_{ij}^v{}^2}_{\text{attracting}} + \underbrace{\frac{1}{N_B} \sum_{i=1}^{N_B} \sum_{j=1}^{N_B} (1 - \omega_{ij}^v) [\gamma - d_{ij}^v]_+^2}_{\text{repelling}}, \quad (8)$$

where N_B denotes the number of samples in each iteration and γ is a margin hyper-parameter. $[x]_+$ denotes $\max(0, x)$, which is a hinge function. Moreover, ω_{ij}^v is the weight term, formulated by a Gaussian kernel function based on the Euclidean distance:

$$\omega_{ij}^v = \exp\left(-\frac{\|f_i^v - f_j^v\|_2^2}{\sigma}\right), \quad (9)$$

where σ represents the kernel bandwidth and $\omega_{ij}^v \in (0, 1]$. Obviously, it can be used to measure the similarity relation of paired samples in the embedding space.

As shown in Eq. (8), the NRL loss contains an attracting term and a repelling term. The positive pairs will approach each other with the help of the attracting term and the repelling term encourages the negative pairs to push away beyond the margin γ .

Similarly, the NRL loss of the infrared modality is defined as:

$$L_{NRL}^r = \underbrace{\frac{1}{N_B} \sum_{i=1}^{N_B} \sum_{j=1}^{N_B} \omega_{ij}^r d_{ij}^r{}^2}_{\text{attracting}} + \underbrace{\frac{1}{N_B} \sum_{i=1}^{N_B} \sum_{j=1}^{N_B} (1 - \omega_{ij}^r) [\gamma - d_{ij}^r]_+^2}_{\text{repelling}}. \quad (10)$$

Therefore, the total loss of the NRL module is:

$$L_{NRL} = L_{NRL}^v + L_{NRL}^r. \quad (11)$$

3.5 Optimal Transport Prototype Matching

The two modules mentioned above primarily concentrate on intra-modality information while overlooking inter-modality connections, which are pivotal in the USVI-ReID task. To this end, following PGM [40] and OTLA [31], we present the Optimal Transport Prototype Matching (OTPM) module to establish reliable cross-modality correspondences at the cluster level. Given the visible prototype set $p^v = \{p_1^v, p_2^v, \dots, p_{Y^v}^v\}$ and the infrared prototype set $p^r = \{p_1^r, p_2^r, \dots, p_{Y^r}^r\}$, where Y^v and Y^r represent the number of visible clusters and infrared clusters, respectively. PGM revealed $Y^v > Y^r$, that is, the number of clusters is inconsistent. In that case, the essence of cross-modality correspondences is the many-to-many matching of inter-modality prototypes, which can be solved

by *Optimal Transport*:

$$\begin{aligned} & \min_Q \langle Q, C \rangle + \frac{1}{\lambda} \mathcal{H}(Q), \\ \text{s.t. } & \begin{cases} Q \mathbb{1} = \mathbb{1} \cdot \frac{1}{Y^v}, \\ Q^T \mathbb{1} = \mathbb{1} \cdot \frac{1}{Y^r}, \end{cases} \end{aligned} \quad (12)$$

where $Q \in \mathbb{R}^{Y^v \times Y^r}$ represents the transport plan for cross-modality matching. $C \in \mathbb{R}^{Y^v \times Y^r}$ is the cost matrix of inter-modality prototypes, i.e., $C_{ij} = 1/\exp(\cos(p_i^v, p_j^r))$, where $\cos(\cdot)$ indicates the cosine similarity. $\langle \cdot \rangle$ denotes the Frobenius dot-product, and $\mathbb{1}$ is an all-one vector. $\mathcal{H}(Q)$ denotes the Entropic Regularization and λ is a regularization parameter. The objective function can be solved by the Sinkhorn-Knopp algorithm [7] and derive the optimal transport plan $Q^* \in \mathbb{R}^{Y^v \times Y^r}$. Then we can obtain two matched pseudo-label sets $Y^{v \rightarrow r}$ and $Y^{r \rightarrow v}$ for network training according to Q^* :

$$\begin{aligned} Y_i^{v \rightarrow r} &= \arg \max_j Q_{ij}^*, j \in \{1, 2, \dots, Y^r\}, \\ Y_j^{r \rightarrow v} &= \arg \max_i Q_{ji}^*, i \in \{1, 2, \dots, Y^v\}. \end{aligned} \quad (13)$$

3.6 Memory Hybrid Learning

We initialize two modality-specific memory banks $\mathcal{M}^v \in \mathbb{R}^{Y^v \times d}$ and $\mathcal{M}^r \in \mathbb{R}^{Y^r \times d}$ by clustering centroids. However, the two modality-specific memories only store the modality-specific information, which can't mine modality-invariant information and reduce the cross-modality discrepancy. To this end, with the cross-modality correspondences derived from the OTPM, we propose a Memory Hybrid Learning (MHL) module to jointly learn modality-specific information and modality-invariant information.

Firstly, we create a modality-hybrid memory $\mathcal{M}^h \in \mathbb{R}^{Y^r \times d}$ to store modality-shared information via mixing matched visible and infrared prototypes by:

$$\begin{aligned} p_i^h &= \alpha \times p_i^r + (1 - \alpha) \times p_i^{r \rightarrow v}, \\ \mathcal{M}_i^h &\leftarrow p_i^h, \end{aligned} \quad (14)$$

where $i \in \{1, 2, \dots, Y^r\}$ and $p_i^{r \rightarrow v}$ denotes the visible prototype which matches with the infrared prototype p_i^r . α is a balancing hyper-parameter that balances the fusion information of the visible and infrared prototypes.

Afterward, during the representation learning stage, we follow the popular memory-based methods [4, 15, 40, 42, 43], which mainly alternate two stages: (1) performing contrastive learning during forward-propagation (FP) and (2) updating the memory during backward-propagation (BP). To better learn the representations, we perform multi-memory joint contrastive learning, which consists of modality-specific contrastive learning and modality-invariant contrastive learning.

Modality-Specific Contrastive Learning. Based on the modality-specific memory \mathcal{M}^v and \mathcal{M}^r , the ClusterNCE [8] loss is applied to learn modality-specific information for network optimization by:

$$L_{MS}^v = -\frac{1}{N_B} \sum_{i=1}^{N_B} \log \frac{\exp(f_i^v \cdot \mathcal{M}^v[\hat{y}_i^v]/\tau)}{\sum_{k=1}^{Y^v} \exp(f_i^v \cdot \mathcal{M}^v[\hat{y}_k^v]/\tau)}, \quad (15)$$

$$L_{MS}^r = -\frac{1}{N_B} \sum_{j=1}^{N_B} \log \frac{\exp(f_j^r \cdot \mathcal{M}^r[\hat{y}_j^r]/\tau)}{\sum_{k=1}^{Y^r} \exp(f_j^r \cdot \mathcal{M}^r[\hat{y}_k^r]/\tau)}, \quad (16)$$

where N_B denotes the number of samples in each iteration. \hat{y}_i^v and \hat{y}_j^r are the pseudo-labels of query features f_i^v and f_j^r . $\mathcal{M}^v[\hat{y}_i^v]$ and $\mathcal{M}^r[\hat{y}_j^r]$ denote the positive representations of query features f_i^v and f_j^r , respectively. Besides, τ is a temperature hyper-parameter. The total loss of modality-specific contrastive learning is:

$$L_{MS} = L_{MS}^v + L_{MS}^r. \quad (17)$$

During the backward-propagation stage, the two modality-specific memories are updated by a momentum update strategy:

$$\mathcal{M}^v[\hat{y}_i^v] \leftarrow \mu \mathcal{M}^v[\hat{y}_i^v] + (1 - \mu) f_i^v, \quad (18)$$

$$\mathcal{M}^r[\hat{y}_j^r] \leftarrow \mu \mathcal{M}^r[\hat{y}_j^r] + (1 - \mu) f_j^r, \quad (19)$$

where μ is the momentum updating factor.

Modality-Invariant Contrastive Learning. Different from two modality-specific memories, we perform modality-invariant contrastive learning on modality-shared memory \mathcal{M}^h to learn modality-invariant information while reducing the cross-modality discrepancy. Following PGM [40], we employ the alternate contrastive learning scheme on \mathcal{M}^h :

$$L_{MI} = \begin{cases} -\frac{1}{N_B} \sum_{i=1}^{N_B} \log \frac{\exp(f_i^v \cdot \mathcal{M}^h[\hat{y}_i^{v \rightarrow r}]/\tau)}{\sum_{k=1}^{Y^r} \exp(f_i^v \cdot \mathcal{M}^h[\hat{y}_k^{v \rightarrow r}]/\tau)}, & \text{if } Epoch\%2 = 0, \\ -\frac{1}{N_B} \sum_{i=1}^{N_B} \log \frac{\exp(f_i^r \cdot \mathcal{M}^h[\hat{y}_i^r]/\tau)}{\sum_{k=1}^{Y^r} \exp(f_i^r \cdot \mathcal{M}^h[\hat{y}_k^r]/\tau)}, & \text{if } Epoch\%2 = 1, \end{cases} \quad (20)$$

where $\hat{y}_i^{v \rightarrow r}$ denotes the visible pseudo-label \hat{y}_i^v matched with the infrared pseudo-label \hat{y}_i^r . Then, the modality-shared memory is updated jointly by query features f_i^v and f_i^r :

$$\begin{aligned} \mathcal{M}^h[\hat{y}_i^{v \rightarrow r}] &\leftarrow \mu \mathcal{M}^v[\hat{y}_i^{v \rightarrow r}] + (1 - \mu) f_i^v, & \text{if } Epoch\%2 = 0, \\ \mathcal{M}^h[\hat{y}_i^r] &\leftarrow \mu \mathcal{M}^r[\hat{y}_i^r] + (1 - \mu) f_i^r, & \text{if } Epoch\%2 = 1. \end{aligned} \quad (21)$$

The total loss of the MHL module is:

$$L_{MHL} = L_{MS} + \beta_1 L_{MI}. \quad (22)$$

3.7 Optimization

The total training loss of the network can be formulated as follows:

$$L = L_{MS} + \beta_1 L_{MI} + \beta_2 L_{NRL}, \quad (23)$$

where β_1, β_2 are balancing coefficients, which are set to 0.5 and 10.0, respectively.

4 EXPERIMENT

4.1 Experiment Setting

Datasets. The proposed method is evaluated on two popular visible-infrared person re-identification datasets: **SYSU-MM01** [37] and **RegDB** [21]. SYSU-MM01 stands as a large-scale, publicly available benchmark tailored for the VI-ReID task, boasting a diverse collection of 491 identities captured across four RGB cameras and two IR cameras, spanning both indoor and outdoor environments. Within this dataset, a total of 22,258 RGB images and 11,909 IR images, portraying 395 distinct identities, have been meticulously curated for training purposes. During the inference phase, the query set encompasses 3,803 IR images, representative of 96 unique identities, while the gallery set comprises 301 randomly selected RGB images. In contrast, the RegDB dataset, captured by a single RGB camera

Table 1: Comparisons with state-of-the-art methods on RegDB and SYSU-MM01, including SVI-ReID, SSVI-ReID, and USVI-ReID methods. All methods are measured by Rank-1 (%) and mAP (%). GUR* denotes the results without camera information.

Settings			RegDB				SYSU-MM01			
			Visible2Thermal		Thermal2Visible		All Search		Indoor Search	
Type	Method	Venue	Rank-1	mAP	Rank-1	mAP	Rank-1	mAP	Rank-1	mAP
SVI-ReID	DDAG [48]	ECCV'20	69.4	63.5	68.1	61.8	54.8	53.0	61.0	68.0
	AGW [49]	TPAMI'21	70.1	66.4	70.5	65.9	47.5	47.7	54.2	63.0
	CAJ [47]	ICCV'21	85.0	79.1	84.8	77.8	69.9	66.9	76.3	80.4
	DART [44]	CVPR'22	83.6	75.7	82.0	73.8	68.7	66.3	72.5	78.2
	LUPI [1]	ECCV'22	88.0	82.7	86.8	81.3	71.1	67.6	82.4	82.7
	DEEN [58]	CVPR'23	91.1	85.1	89.5	83.4	74.7	71.8	80.3	83.3
	PartMix [16]	CVPR'23	85.7	82.3	84.9	82.5	77.8	74.6	81.5	84.4
	ProtoHPE [54]	MM'23	88.7	83.7	88.7	82.0	71.9	70.6	77.8	81.3
	SAAI [10]	ICCV'23	91.1	91.5	92.1	92.0	75.9	77.0	83.2	88.0
	PMWGCN [28]	TIFS'24	90.6	84.5	88.8	81.6	66.8	64.9	72.6	76.2
	LCNL [45]	IJCV'24	85.6	78.7	84.0	76.9	70.2	68.0	76.2	80.3
SSVI-ReID	OTLA [31]	ECCV'22	48.2	43.9	47.4	56.8	49.9	41.8	49.6	42.8
	TAA [41]	TIP'23	62.2	56.0	63.8	56.5	48.8	42.3	50.1	56.0
	DPIs [26]	ICCV'23	62.3	53.2	61.5	52.7	58.4	55.6	63.0	70.0
USVI-ReID	OTLA [31]	ECCV'22	32.9	29.7	32.1	28.6	29.9	27.1	29.8	38.8
	ADCA [43]	MM'22	67.2	64.1	68.5	63.8	45.5	42.7	50.6	59.1
	CHCR [22]	TCSVT'23	68.2	63.8	70.0	65.9	47.7	45.3	-	-
	DOTLA [4]	MM'23	85.6	76.7	82.9	75.0	50.4	47.4	53.5	61.7
	MBCCM [15]	MM'23	83.8	77.9	82.8	76.7	53.1	48.2	55.2	62.0
	CCLNet [3]	MM'23	69.9	65.5	70.2	66.7	54.0	50.2	56.7	65.1
	PGM [40]	CVPR'23	69.5	65.4	69.9	65.2	57.3	51.8	56.2	62.7
	GUR* [42]	ICCV'23	73.9	70.2	75.0	69.9	61.0	57.0	64.2	69.5
	RPNR	Ours	90.9	84.7	90.1	83.2	65.2	60.0	68.9	74.4

and a single IR camera, features 4,120 RGB images and 4,120 IR images, each depicting 412 distinct identities. To elaborate further, the dataset is partitioned into two disjoint sets: one designated for training and the other for testing.

Evaluation Metrics. The experiment of our method was carried out following the evaluation metrics in DDAG [48], i.e., Cumulative Matching Characteristic (CMC) and Mean Average Precision (mAP). In the evaluation of our proposed method on the SYSU-MM01 dataset, we consider two distinct search modes: the All Search mode and the Indoor Search mode. Similarly, for the RegDB dataset, our method is evaluated across two testing modes: Visible2Thermal and Thermal2Visible.

Implementation Details. The proposed method is implemented on two TITAN RTX GPUs with PyTorch. During the training stage, all the input images are resized to 288×144, and data augmentations described in [47] are adopted for image augmentation. Following [49], we employ a two-stream feature extractor pre-trained on ImageNet to extract 2048-dimensional features of input images. The Adam optimizer is adopted to train the network with a weight decay of 5e-4. The initial learning rate is set to 3.5e-4, which decays to 1/10 of its previous value every 20 epochs. The number of training epochs is set to 100. In the first 50 epochs, we employ the

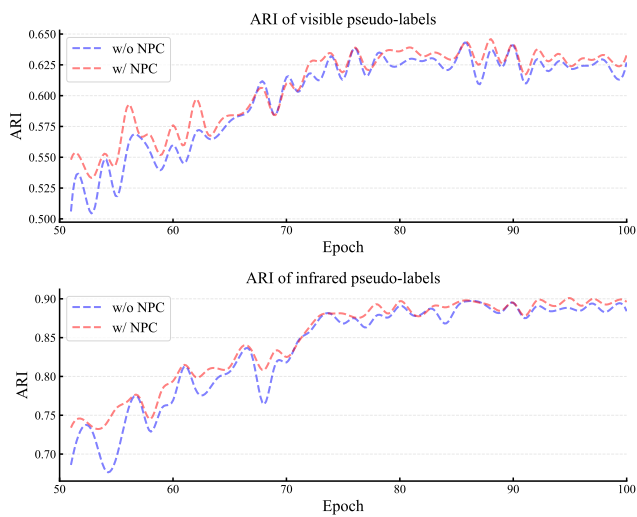
DCL [43] framework to alternately offline pseudo-labels generation and online representation learning. The proposed framework is trained in the last 50 epochs. Additionally, we store multiple proxies for each cluster to provide complementary representation at each stage when constructing the memory following [39, 61]. The parameter κ for κ -reciprocal nearest neighbors in Eq. (1) is set to 30 following [60] and K in Eq. (3) is fixed to 20. The hyper-parameter λ in Eq. (12) is set to 25 following [31]. Following ADCA [43], the momentum value μ is set to 0.1 and the temperature τ is 0.5. The margin hyper-parameter γ in Eq. (8) and the kernel bandwidth σ in Eq. (9) are both set to 1.0 following [17]. The trade-off hyper-parameter α in Eq. (14) is set to 0.5, β_1 and β_2 in Eq. (23) is set to 0.5 and 10.0, respectively.

4.2 Comparison with State-of-the-art Methods

To comprehensively illustrate the efficiency of our method, we compare our method with three typical related methods: (1) supervised visible-infrared person ReID (SVI-ReID), (2) semi-supervised visible-infrared person ReID (SSVI-ReID), and (3) unsupervised visible-infrared person ReID (USVI-ReID). If not specified, we conduct analysis on SYSU-MM01 under the All Search mode.

Table 2: Ablation studies on SYSU-MM01 under the All Search mode and Indoor Search mode. Rank-R accuracy(%) and mAP(%) are reported.

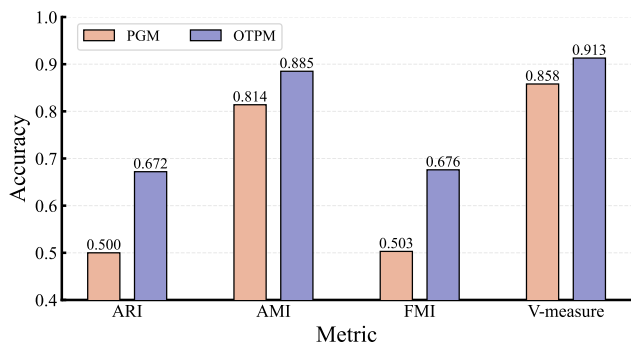
Order	Module					All Search		Indoor Search	
	Baseline	NPC	NRL	OTPM	MHL	Rank-1	mAP	Rank-1	mAP
1	✓					40.4	39.0	42.3	51.2
2	✓	✓				41.2	39.5	43.6	52.0
3	✓		✓			42.5	41.4	45.5	53.9
4	✓	✓	✓			44.6	42.2	46.7	54.5
5	✓			✓	✓	60.2	55.8	62.9	69.3
6	✓	✓		✓	✓	62.5	57.1	64.2	70.3
7	✓		✓	✓	✓	63.7	57.4	64.7	70.5
8	✓	✓	✓	✓	✓	65.2	60.0	68.9	74.4

**Figure 2: The ARI metric of visible and infrared pseudo-labels on SYSU-MM01 at each epoch.**

Comparison with SVI-ReID Methods. Compared to SVI-ReID methods that rely on high-quality cross-modality annotations, the results of our RPNR are promising. As we can see, our method achieves comparable performance to some supervised methods (e.g., DDAG [48], AGW [49], and CAJ [47]), which is attributed to the fact that our proposed method can provide reliable pseudo-labels for unsupervised tasks.

Comparison with SSVI-ReID Methods. Several SSVI-ReID methods have been proposed to mitigate the issue of the high cost of cross-modality annotations. These methods utilize partial annotations to accomplish the VI-ReID task. It is noteworthy that our approach, without any cross-modality annotations, achieves a 6.8% improvement in Rank-1 and a 4.4% improvement in mAP on the SYSU-MM01 dataset compared to the SOTA DPIS method.

Comparison with USVI-ReID Methods. As shown in Tab. 1, our method significantly outperforms existing state-of-the-art USVI-ReID methods. To be specific, our RPNR achieves 65.2% in Rank-1 and 60.0% in mAP on SYSU-MM01, which surpasses SOTA GUR by 4.2% in Rank-1 and 3.0% in mAP. Surprisingly, the performance

**Figure 3: The accuracy of cross-modality correspondences compared with PGM [40] on SYSU-MM01.**

on RegDB achieves 90.9% in Rank-1 and 84.7% in mAP under the Visible2Thermal mode, which outperforms SOTA GUR by a large margin of 17.0% in Rank-1 and 14.5% in mAP. The results powerfully demonstrate the effectiveness of our approach, highlighting that our RPNR provides more reliable pseudo-labels and establishes more dependable cross-modality correspondences for USVI-ReID.

4.3 Ablation Study

To validate the effectiveness of each module in the RPNR, we conduct ablation experiments on SYSU-MM01. The results are shown in Tab. 2. We employ the DCL framework with multiple proxies as the baseline.

Effectiveness of the NPC Module. The NPC module is proposed to explicitly rectify noisy pseudo-labels to obtain more reliable pseudo-labels. As shown in Order 5 and Order 6 in Tab. 2, the performance of Order 6 with NPC improves by about 2% compared to Order 5. To more clearly demonstrate the effectiveness of the NPC module, we utilize the Adjusted Rand Index (ARI) metric to evaluate the accuracy of visible and infrared pseudo-labels on SYSU-MM01 at each epoch. A higher ARI value indicates more accurate pseudo-labels. As depicted in Fig. 2, the introduction of the NPC module results in improved accuracies for both visible and infrared pseudo-labels, thereby providing more reliable pseudo-labels for network training.

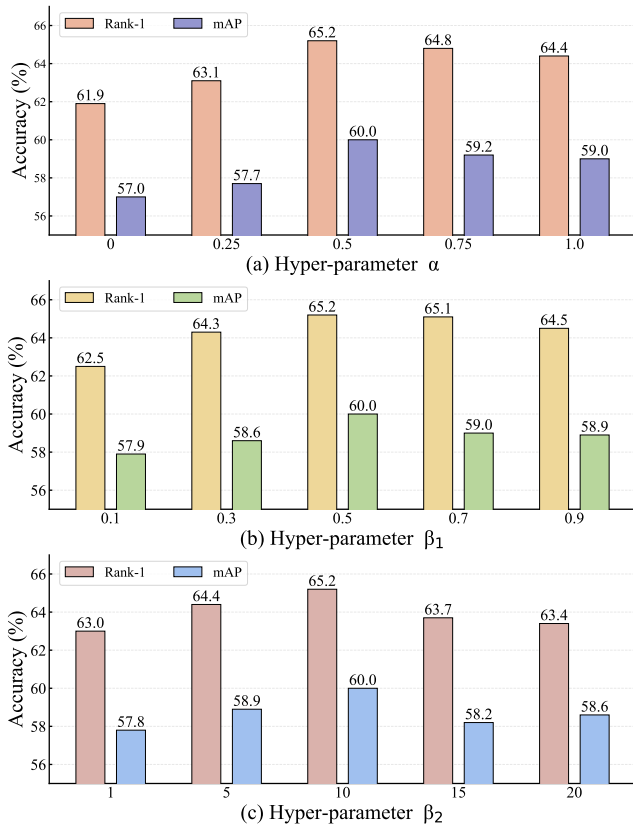


Figure 4: The influence of three import hyper-parameters with different values on SYSU-MM01.

Effectiveness of the NRL Module. The NRL module is introduced as complementary information to make up for the shortcomings of rigid pseudo-labels. After adding the NRL module, the performance can gain improvement by 2%-4% in Rank-1 on SYSU-MM01. It shows that the NRL module can explore meaningful intricate interactions spanning across all pair-wise samples to provide complementary supervision information for the network.

Effectiveness of the OTPM Module. As shown in Fig. 3, we compared the cross-modality matching accuracy of OTPM with that of PGM on four clustering evaluation metrics to show the effectiveness of OTPM. As we can see, OTPM significantly outperforms the PGM on all four metrics, indicating its superior ability to establish reliable cross-modality correspondences at the cluster level.

Effectiveness of the MHL Module. We present the MHL module to jointly learn modality-specific and modality-invariant information while reducing cross-modality discrepancies. Note that the MHL module cannot be executed on its own, as it is built on top of the OTPM module. Compared to the Baseline, the combination of MHL with OTPM leads to a significant performance improvement, with a large margin of 19.8% in Rank-1 accuracy and 16.8% in mAP (See Order 1 & Order 5). This highlights the efficiency of MHL in leveraging modality-specific and modality-invariant information, effectively mitigating cross-modality discrepancies.

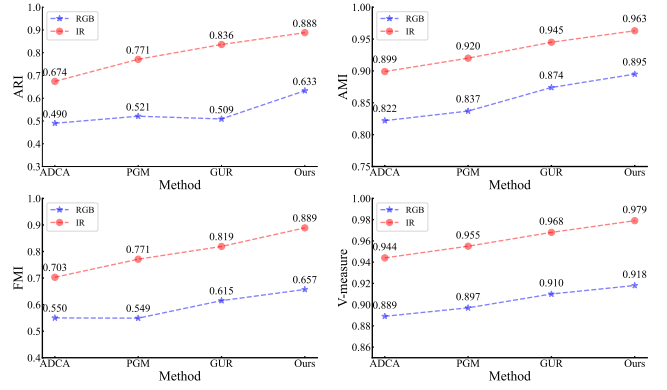


Figure 5: Four clustering evaluation metrics compared with state-of-the-art methods on the SYSU-MM01 dataset. “RGB” and “IR” denote the accuracy of visible and infrared pseudo-labels, respectively.

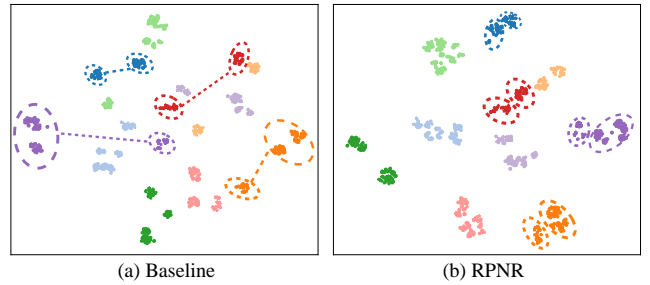


Figure 6: The t-SNE visualization of randomly chosen 10 identities, with each identity represented by a distinct color and each modality denoted by different shapes.

4.4 Further Analysis

Hyper-parameter Analysis. There are three key hyper-parameters in our method, and we give the quantitative results to evaluate their influence with different values in Fig. 4. As we can see, the best performance is achieved when α is set to 0.5, β_1 is set to 0.5, and β_2 is set to 10.0, respectively.

Accuracy of Pseudo-labels. As shown in Fig. 5, we compared our method with several SOTA USVI-ReID methods on four common clustering metrics to show the effectiveness of the proposed RPNR. The results show that the visible and infrared pseudo-labels generated by RPNR significantly outperform existing methods on all four clustering metrics, indicating that our method provides more reliable pseudo-labels for network training, thereby boosting performance improvement.

Visualization Analysis. We visualize the visible and infrared feature distribution with t-SNE in the 2-D embedding space, which contains 10 randomly selected identities. As shown in Fig. 6, compared to the Baseline, in our approach, the feature distributions of the same identities from the same modality are more compact (see orange and purple circles), and the feature distributions of the same identities from different modalities are also closer (see red and blue circles). This indicates that RPNR significantly reduces

cross-modality disparities and establishes a solid foundation for reliable cross-modality correspondences.

5 CONCLUSION

In this paper, we introduce an effective approach for addressing the USVI-ReID task, termed Robust Pseudo-label Learning with Neighbor Relation (RPNR). Our goal is to explore more reliable pseudo-labels and establish more dependable cross-modality correspondences for the USVI-ReID task. To this end, we first employ the Noisy Pseudo-label Calibration module to rectify noisy pseudo-labels, thereby obtaining more reliable pseudo-labels. Subsequently, we present the Neighbor Relation Learning module to model the potential interactions between different samples. In addition, we introduce the Optimal Transport Prototype Matching module to establish dependable cross-modality correspondences at the cluster level. Finally, we propose the Memory Hybrid Learning module to mine modality-specific and modality-invariant information while mitigating significant cross-modality disparities. Comprehensive experimental results on two popular benchmarks demonstrate the effectiveness of the proposed method.

REFERENCES

- [1] Mahdi Alehdaghi, Arthur Josi, Rafael M. O. Cruz, and Eric Granger. 2022. Visible-Infrared Person Re-Identification Using Privileged Intermediate Information. In *ECCV*. 720–737.
- [2] Xinlei Chen and Abhinav Gupta. 2015. Webly supervised learning of convolutional networks. In *ICCV*. 1431–1439.
- [3] Zhong Chen, Zhizhong Zhang, Xin Tan, Yanyun Qu, and Yuan Xie. 2023. Unveiling the Power of CLIP in Unsupervised Visible-Infrared Person Re-Identification. In *ACM MM*. 3667–3675.
- [4] De Cheng, Xiaojian Huang, Nannan Wang, Lingfeng He, Zhihui Li, and Xinbo Gao. 2023. Unsupervised Visible-Infrared Person ReID by Collaborative Learning with Neighbor-Guided Label Refinement. (2023).
- [5] De Cheng, Haichun Tai, Nannan Wang, Zhen Wang, and Xinbo Gao. 2022. Neighbour consistency guided pseudo-label refinement for unsupervised person re-identification. *arXiv preprint arXiv:2211.16847* (2022).
- [6] Yoonki Cho, Woo Jae Kim, Seunghoon Hong, and Sung-Eui Yoon. 2022. Part-based Pseudo Label Refinement for Unsupervised Person Re-identification. In *CVPR*. 7298–7308.
- [7] M Cuturi. 2013. Lightspeed computation of optimal transportation distances. *Advances in Neural Information Processing Systems* 26, 2 (2013), 2292–2300.
- [8] Zuozhuo Dai, Guangyuan Wang, Weihao Yuan, Siyu Zhu, and Ping Tan. 2022. Cluster Contrast for Unsupervised Person Re-identification. In *ACCV*. 319–337.
- [9] Martin Ester, Hans-Peter Kriegel, Jörg Sander, and Xiaowei Xu. 1996. A Density-Based Algorithm for Discovering Clusters in Large Spatial Databases with Noise. In *KDD*. 226–231.
- [10] Xingye Fang, Yang Yang, and Ying Fu. 2023. Visible-Infrared Person Re-Identification via Semantic Alignment and Affinity Inference. In *ICCV*. 11270–11279.
- [11] Jiawei Feng, Ancong Wu, and Wei-Shi Zheng. 2023. Shape-Erased Feature Learning for Visible-Infrared Person Re-Identification. In *CVPR*. 22752–22761.
- [12] Yixiao Ge, Dapeng Chen, and Hongsheng Li. 2020. Mutual Mean-Teaching: Pseudo Label Refinery for Unsupervised Domain Adaptation on Person Re-identification. In *ICLR*.
- [13] Bo Han, Quanming Yao, Xingrui Yu, Gang Niu, Miao Xu, Weihua Hu, Ivor Tsang, and Masashi Sugiyama. 2018. Co-teaching: Robust training of deep neural networks with extremely noisy labels. *Advances in neural information processing systems* 31 (2018).
- [14] Jiangfan Han, Ping Luo, and Xiaogang Wang. 2019. Deep self-learning from noisy labels. In *ICCV*. 5138–5147.
- [15] Lingfeng He, Nannan Wang, Shizhou Zhang, Zhen Wang, Xinbo Gao, et al. 2023. Efficient Bilateral Cross-Modality Cluster Matching for Unsupervised Visible-Infrared Person ReID. (2023).
- [16] Minsu Kim, Seungrong Kim, Jungin Park, Seongheon Park, and Kwanghoon Sohn. 2023. PartMix: Regularization Strategy to Learn Part Discovery for Visible-Infrared Person Re-Identification. In *CVPR*. 18621–18632.
- [17] Sungyeon Kim, Dongwon Kim, Minsu Cho, and Suha Kwak. 2021. Embedding transfer with label relaxation for improved metric learning. In *CVPR*. 3967–3976.
- [18] Jichang Li, Guanbin Li, Feng Liu, and Yizhou Yu. 2022. Neighborhood collective estimation for noisy label identification and correction. In *ECCV*. 128–145.
- [19] Junnan Li, Richard Socher, and Steven CH Hoi. 2020. Dividemix: Learning with noisy labels as semi-supervised learning. *arXiv preprint arXiv:2002.07394* (2020).
- [20] Huafeng Liu, Mengmeng Sheng, Zeren Sun, Yazhou Yao, Xian-Sheng Hua, and Heng-Tao Shen. 2024. Learning with Imbalanced Noisy Data by Preventing Bias in Sample Selection. *arXiv preprint arXiv:2402.11242* (2024).
- [21] Dat Tien Nguyen, Hyung Gil Hong, Ki-Wan Kim, and Kang Ryoung Park. 2017. Person Recognition System Based on a Combination of Body Images from Visible Light and Thermal Cameras. *Sensors* 17, 3 (2017), 605.
- [22] Zhiqi Pang, Chunyu Wang, Lingling Zhao, Yang Liu, and Gaurav Sharma. 2023. Cross-modality Hierarchical Clustering and Refinement for Unsupervised Visible-Infrared Person Re-Identification. *IEEE Transactions on Circuits and Systems for Video Technology* (2023).
- [23] Jiangming Shi, Xiangbo Yin, Yeyun Chen, Yachao Zhang, Zhizhong Zhang, Yuan Xie, and Yanyun Qu. 2024. Multi-Memory Matching for Unsupervised Visible-Infrared Person Re-Identification. *arXiv preprint arXiv:2401.06825* (2024).
- [24] Jiangming Shi, Xiangbo Yin, Yaoxing Wang, Xiaofeng Liu, Yuan Xie, and Yanyun Qu. 2024. Progressive Contrastive Learning with Multi-Prototype for Unsupervised Visible-Infrared Person Re-identification. *arXiv preprint arXiv:2402.19026* (2024).
- [25] Jiangming Shi, Xiangbo Yin, Demao Zhang, and Yanyun Qu. 2023. Visible Embraces Infrared: Cross-Modality Person Re-Identification with Single-Modality Supervision. In *2023 China Automation Congress (CAC)*. 4781–4787.
- [26] Jiangming Shi, Yachao Zhang, Xiangbo Yin, Yuan Xie, Zhizhong Zhang, Jianping Fan, Zhongchao Shi, and Yanyun Qu. 2023. Dual Pseudo-Labels Interactive Self-Training for Semi-Supervised Visible-Infrared Person Re-Identification. In *ICCV*. 11218–11228.
- [27] Hwanjun Song, Minseok Kim, and Jae-Gil Lee. 2019. Selfie: Refurbishing unclean samples for robust deep learning. In *ICML*. 5907–5915.
- [28] Rui Sun, Long Chen, Lei Zhang, Ruirui Xie, and Jun Gao. 2024. Robust Visible-Infrared Person Re-Identification based on Polymorphic Mask and Wavelet Graph Convolutional Network. *IEEE Transactions on Information Forensics and Security* (2024).
- [29] Zeren Sun, Xian-Sheng Hua, Yazhou Yao, Xiu-Shen Wei, Guosheng Hu, and Jian Zhang. 2020. Crssc: salvage reusable samples from noisy data for robust learning. In *MM*. 92–101.
- [30] Daiki Tanaka, Daiki Ikami, Toshihiko Yamasaki, and Kiyoharu Aizawa. 2018. Joint optimization framework for learning with noisy labels. In *CVPR*. 5552–5560.
- [31] Jiangming Wang, Zhizhong Zhang, Mingang Chen, Yi Zhang, Cong Wang, Bin Sheng, Yanyun Qu, and Yuan Xie. 2022. Optimal Transport for Label-Efficient Visible-Infrared Person Re-Identification. In *ECCV*. 93–109.
- [32] Menglin Wang, Baisheng Lai, Jianqiang Huang, Xiaojin Gong, and Xian-Sheng Hua. 2021. Camera-Aware Proxies for Unsupervised Person Re-Identification. In *AAAI*. 2764–2772.
- [33] Pengfei Wang, Changxing Ding, Wentao Tan, Mingming Gong, Kui Jia, and Dacheng Tao. 2022. Uncertainty-aware clustering for unsupervised domain adaptive object re-identification. *IEEE Transactions on Multimedia* (2022).
- [34] Yuhao Wang, Xuehu Liu, Pingping Zhang, Hu Lu, Zhengzheng Tu, and Huchuan Lu. 2024. TOP-ReID: Multi-spectral Object Re-Identification with Token Permutation. In *AAAI*. 5758–5766.
- [35] Hongxin Wei, Lei Feng, Xiangyu Chen, and Bo An. 2020. Combating noisy labels by agreement: A joint training method with co-regularization. In *CVPR*. 13726–13735.
- [36] Jiayu Jiang Fei Wang Yibing Zhan Dapeng Tao Wentao Tan, Changxing Ding. 2024. Harnessing the Power of MLLMs for Transferable Text-to-Image Person ReID. *CVPR* (2024).
- [37] Ancong Wu, Wei-Shi Zheng, Hong-Xing Yu, Shaogang Gong, and Jianhuang Lai. 2017. RGB-Infrared Cross-Modality Person Re-identification. In *ICCV*. 5390–5399.
- [38] Jianbing Wu, Hong Liu, Yuxin Su, Wei Shi, and Hao Tang. 2023. Learning Concordant Attention via Target-aware Alignment for Visible-Infrared Person Re-identification. In *ICCV*. 11122–11131.
- [39] Yuhang Wu, Tengting Huang, Haotian Yao, Chi Zhang, Yuanjie Shao, Chuchu Han, Changxin Gao, and Nong Sang. 2022. Multi-Centroid Representation Network for Domain Adaptive Person Re-ID. In *AAAI*. 2750–2758.
- [40] Zesen Wu and Mang Ye. 2023. Unsupervised Visible-Infrared Person Re-Identification via Progressive Graph Matching and Alternate Learning. In *CVPR*. 9548–9558.
- [41] Bin Yang, Jun Chen, Xianzheng Ma, and Mang Ye. 2023. Translation, Association and Augmentation: Learning Cross-Modality Re-Identification From Single-Modality Annotation. *IEEE Transactions on Image Processing* 32 (2023), 5099–5113.
- [42] Bin Yang, Jun Chen, and Mang Ye. 2023. Towards Grand Unified Representation Learning for Unsupervised Visible-Infrared Person Re-Identification. In *ICCV*. 11069–11079.
- [43] Bin Yang, Mang Ye, Jun Chen, and Zesen Wu. 2022. Augmented Dual-Contrastive Aggregation Learning for Unsupervised Visible-Infrared Person Re-Identification. In *ACM MM*. 2843–2851.

- [44] Mouxing Yang, Zhenyu Huang, Peng Hu, Taihao Li, Jiancheng Lv, and Xi Peng. 2022. Learning with Twin Noisy Labels for Visible-Infrared Person Re-Identification. In *CVPR*. 14288–14297.
- [45] Mouxing Yang, Zhenyu Huang, and Xi Peng. 2024. Robust object re-identification with coupled noisy labels. *International Journal of Computer Vision* (2024), 1–19.
- [46] Yazhou Yao, Zeren Sun, Chuanyi Zhang, Fumin Shen, Qi Wu, Jian Zhang, and Zhenmin Tang. 2021. Jo-src: A contrastive approach for combating noisy labels. In *CVPR*. 5192–5201.
- [47] Mang Ye, Weijian Ruan, Bo Du, and Mike Zheng Shou. 2021. Channel Augmented Joint Learning for Visible-Infrared Recognition. In *ICCV*. 13547–13556.
- [48] Mang Ye, Jianbing Shen, David J. Crandall, Ling Shao, and Jiebo Luo. 2020. Dynamic Dual-Attentive Aggregation Learning for Visible-Infrared Person Re-identification. In *ECCV*. 229–247.
- [49] Mang Ye, Jianbing Shen, Gaojie Lin, Tao Xiang, Ling Shao, and Steven C. H. Hoi. 2022. Deep Learning for Person Re-Identification: A Survey and Outlook. *IEEE Trans. Pattern Anal. Mach. Intell.* (2022), 2872–2893.
- [50] Kun Yi and Jianxin Wu. 2019. Probabilistic end-to-end noise correction for learning with noisy labels. In *CVPR*. 7017–7025.
- [51] Chenyang Yu, Xuehu Liu, Yingquan Wang, Pingping Zhang, and Huchuan Lu. 2024. TF-CLIP: Learning Text-Free CLIP for Video-Based Person Re-identification. In *AAAI*. 6764–6772.
- [52] Hao Yu, Xu Cheng, Wei Peng, Weihao Liu, and Guoying Zhao. 2023. Modality Unifying Network for Visible-Infrared Person Re-Identification. In *ICCV*. 11185–11195.
- [53] Guoqing Zhang, Hongwei Zhang, Weisi Lin, Arun Kumar Chandran, and Xuan Jing. 2023. Camera Contrast Learning for Unsupervised Person Re-Identification. *IEEE Trans. Circuits Syst. Video Technol.* 33, 8 (2023), 4096–4107.
- [54] Guiwei Zhang, Yongfei Zhang, and Zichang Tan. 2023. ProtoHPE: Prototype-guided High-frequency Patch Enhancement for Visible-Infrared Person Re-identification. In *MM*. 944–954.
- [55] Pingping Zhang, Yuhao Wang, Yang Liu, Zhengzheng Tu, and Huchuan Lu. 2024. Magic tokens: Select diverse tokens for multi-modal object re-identification. *CVPR* (2024).
- [56] Xiao Zhang, Yixiao Ge, Yu Qiao, and Hongsheng Li. 2021. Refining pseudo labels with clustering consensus over generations for unsupervised object re-identification. In *CVPR*. 3436–3445.
- [57] Xinyu Zhang, Dongdong Li, Zhigang Wang, Jian Wang, Errui Ding, Javen Qinfeng Shi, Zhaoxiang Zhang, and Jingdong Wang. 2022. Implicit Sample Extension for Unsupervised Person Re-Identification. In *CVPR*. 7359–7368.
- [58] Yukang Zhang and Hanzi Wang. 2023. Diverse Embedding Expansion Network and Low-Light Cross-Modality Benchmark for Visible-Infrared Person Re-identification. In *CVPR*. 2153–2162.
- [59] Yikai Zhang, Songzhu Zheng, Pengxiang Wu, Mayank Goswami, and Chao Chen. 2021. Learning with feature-dependent label noise: A progressive approach. *arXiv preprint arXiv:2103.07756* (2021).
- [60] Zhun Zhong, Liang Zheng, Donglin Cao, and Shaozi Li. 2017. Re-ranking person re-identification with k-reciprocal encoding. In *CVPR*. 1318–1327.
- [61] Chang Zou, Zeqi Chen, Zhichao Cui, Yuehu Liu, and Chi Zhang. 2023. Discrepant and Multi-Instance Proxies for Unsupervised Person Re-Identification. In *ICCV*. 11058–11068.
- [62] Jialong Zuo, Changqian Yu, Nong Sang, and Changxin Gao. 2023. PliP: Language-image pre-training for person representation learning. *arXiv preprint arXiv:2305.08386* (2023).
- [63] Jialong Zuo, Hanyu Zhou, Ying Nie, Feng Zhang, Tianyu Guo, Nong Sang, Yunhe Wang, and Changxin Gao. 2024. UFineBench: Towards Text-based Person Retrieval with Ultra-fine Granularity. *CVPR* (2024).